A Comparison of Newtonian and Viscoelastic Constitutive Models for Dry Spinning of Polymer Fibers

Zeming Gou, Anthony J. McHugh

Department of Chemical Engineering, University of Illinois at Urbana–Champaign, 600 South Mathews Avenue, Urbana, Illinois 61801

Received 13 November 2001; accepted 4 March 2002

ABSTRACT: A comparison is made of the predictions of one-dimensional mathematical model simulations of dry spinning based on Newtonian and viscoelastic constitutive equations for the spin dope. The viscoelastic model is based upon a modified Giesekus constitutive equation with a temperature and composition-dependent relaxation time. The simulation algorithm includes the effects of the glass transition on the expected solution viscosity and relaxation time behavior along the spinline. Predictions of axial velocity, tensile stress, and composition profiles for the two cases suggest the role of viscoelasticity in the locking-in behavior associated with fiber solidification along the spinline. The effects of model parameters and processing conditions are also discussed. © 2003 Wiley Periodicals, Inc. J Appl Polym Sci 87: 2136–2145, 2003

Key words: fibers; modeling; viscoelastic properties; glass transition

INTRODUCTION

Dry spinning is an important fiber-spinning process used in cases where the polymer may be susceptible to thermal degradation or where certain surface characteristics of the filaments are desired. It is widely used for the manufacture of fibers from cellulose acetate, cellulose triacetate, polymers and copolymers of vinyl chloride, acrylonitrile, and others. More recently, dry spinning has been used as an intermediate step in the production of high strength fibers of nylon[1] and polylactide[2] from various spinning solutions. The added feature of composition changes due to solvent evaporation along the spinline makes dry spinning more complicated than melt spinning, both in terms of its technical realization and the physical mechanisms involved in the solidification process. Despite its commercial importance, however, dry spinning has received very little attention in the literature in recent years, particularly with regard to modeling studies.

Analysis of dry spinning requires the formulation of a system of three simultaneous equations, describing the momentum, energy, and mass transfer, in combination with a constitutive equation for the concentrated solution. One wishes to predict the fiber velocity, temperature, composition, and tensile stress profiles at points along the spinline, including the take-up roll, as well as the solidification point, where stresses are expected to correlate with the fiber properties. Because concentrated polymeric solutions exhibit viscoelastic behavior rather than purely viscous behavior,[3] viscoelasticity would be expected to play an important role in the dry spinning processes that should also be incorporated in the model. The prediction of effects such as skinning and its relation to the formation of crenulated structures in the as-spun fibers would require two-dimensional models to capture effects related to the radial variation of the temperature and concentration profiles. However, before such considerations can be made, one needs a robust one-dimensional model that is capable of capturing the major features mentioned above.

Previous efforts at mathematical modeling focused on the use of purely viscous constitutive equations in one-dimensional formulations along with various simplifications in the integration schemes used. Initial efforts were made by Griskey and Fok,[4,5] who utilized experimental values of radially averaged concentration in solving the partial differential equation representing the solvent material balance. A more comprehensive one-dimensional model for several polymer/solvent systems was published by Ohzawa et al.,[6–8] who assumed that tension was constant along the length of the spinline. Ziabicki[3] has also given an extensive discussion of the mechanisms in dry spinning. Brazinsky et al.[9] compared their theoretical calculations based on a two-dimensional mathematical model of cellulose acetate/acetone dry spinning with experimental data. The variation of tension with axial position and the die swell of the filament leaving the

Correspondence to: A. J. McHugh (a-mchugh@uiuc.edu).

Contract grant sponsor: ERC program of the National Science Foundation; contract grant number: EEC-9731680.

Journal of Applied Polymer Science, Vol. 87, 2136–2145 (2003)

spinneret hole were taken into consideration. Ishihara et al.[10] carried out a modeling endeavor for dry spinning of polyurethane–urea elastomers with the consideration of deflection. More recently, Zhou[11] established a mathematical model for the dry spinning process of hollow filaments, using polyacrylonitrile (PAN)–dimethylformamide (DMF) solution as an example material. As noted, in all of the previous work described above, purely viscous constitutive models, either a Newtonian constitutive equation[6–10] or a modified Cross model,[11] with composition-dependent rheologic parameters, were chosen. Moreover, these models only consider early-stage behavior, prior to solidification, which is another very important issue. Solidification, i.e., the transformation of a spinning fluid into a solid polymer, involves irreversible changes in structural and macroscopic characteristics of the material. Understanding the solidification mechanism and prediction of the solidification point are very important issues in the modeling of dry spinning. However, to our knowledge, there are no published dry spinning models that consider the viscoelastic rheologic properties of the dry spinning solutions, nor has there been a model treatment that explicitly accounts for a solidification mechanism to lock in the polymer system. The purpose of this article is to present a generic one-dimensional model of dry spinning that includes viscoelasticity as well as a mechanism for solidification and to compare predictions of this model with those based on the assumptions of Newtonian behavior.

MODEL DEVELOPMENT

The equations that comprise the model are essentially divided into three general categories: transport balance equations for momentum, energy and mass, constitutive equations, and correlations for material properties. In the following development, subscripts (1) and (2) will refer, respectively to the polymer and solvent.

Transport balances

The dry spinning process shown schematically in Figure 1 illustrates the process variables and boundary conditions. An axisymmetric stream of spin dope exits a spinneret of diameter d_o at a mass flow rate W, and temperature T_o, and is drawn continuously at a take-up speed v_L. The volume fraction of solvent in the spin dope is ϕ_{20}. Air is pumped from the bottom end of the cabinet at velocity v_a and temperature T_a, and exits from the top end of the cabinet with the evaporated solvent. The solvent evaporation process in the cabinet is indicated by the mass flux of solvent relative to the mass average velocity at the fiber surface $j_2|_R$. In industrial practice the spinneret has a multitude of holes; however, in this study, as is the usual practice, a single filament approximation is used. Due to the similarity between dry spinning and melt spinning, a number of fundamental assumptions and methodologies used in melt spinning modeling[12] can also be applied in the development of our dry spinning model. More details on the equation derivations are given elsewhere.[13]

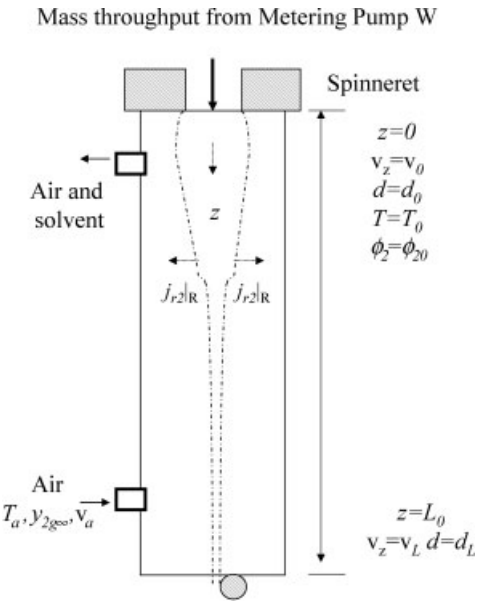

Figure 1 Schematic representation of the dry spinning process, illustrating process variables and boundary conditions.

Equation of continuity

Following the usual practice,[3] solvent evaporation on the gas film side is expressed in terms of a mass transfer coefficient formalism and ideal solution behavior in the filament (i.e., no volume changes on mixing), ideal gas behavior on the air side, and gas–liquid equilibrium at the air–fiber interface are also assumed. The steady-state mass balance equation for the filament is derived by integrating the continuity equation across the fiber cross section (assumed circular), leading to the following result for the axial (z) variation of the solvent composition in the fiber[3,13]

$$\frac{d\phi_2}{dz} + \frac{2\hat{v}_2 k_y M_2(1-\phi_2)}{Rv_z}\left(\frac{a_2 P_2^{\text{sat}} - P y_{2_{g^\infty}}}{P - a_2 P_2^{\text{sat}}}\right) = 0 \quad (1)$$

In this expression, ϕ_2 is the volume fraction of solvent, ν_2 is the solvent partial specific volume, k_y is the gas film-side mass transfer coefficient, M_2 is the solvent molecular weight, P is the total pressure, P_2^{sat} is the pure solvent vapor pressure, R is the filament radius, y_{2g^∞} is the solvent mol fraction in the bulk gas phase, v_z is the axial velocity, and a_2 is the solvent activity on the polymer film side. The spinline radius is related to

the mass flow rate through the overall material balance,

$$R = \left(\frac{W_1 \hat{\nu}_1}{\pi(1 - \phi_2) v_z} \right)^{1/2}. \quad (2)$$

Equation of motion

The 1D momentum balance is obtained by integrating the cylindrical coordinate r and z components of the equations of motion across the fiber radius. One assumes the flow field during dry spinning is locally homogeneous, uniaxial extension, and that inertia due to the solvent evaporation,[3] and die swell are negligible. Thus, the velocity gradient tensor $\nabla \mathbf{v}$ has the form

$$\nabla \mathbf{v} = \begin{bmatrix} \frac{dv_z}{dz} & 0 & 0 \\ 0 & -\frac{1}{2}\frac{dv_z}{dz} & 0 \\ 0 & 0 & -\frac{1}{2}\frac{dv_z}{dz} \end{bmatrix} \quad (3)$$

The assumption of axial symmetry also implies a diagonal extra stress tensor of the form

$$\boldsymbol{\tau} = \begin{bmatrix} \tau_{zz} & 0 & 0 \\ 0 & \tau_{rr} & 0 \\ 0 & 0 & \tau_{\theta\theta} \end{bmatrix} \quad (4)$$

where the rr and $\theta\theta$ components are equal.

One of the differences between dry spinning and melt spinning is the air drag effect because of the mass transfer of solvent between the outer layer of filament and the medium air, which causes a change in the thickness of the boundary layer.[14] Under the assumptions above, the equation that is often used in melt spinning process[12] also results for dry spinning with a change in the air drag term.

$$\rho A v_z \frac{dv_z}{dz} = \frac{d}{dz}[A(\tau_{zz} - \tau_{rr})] - \pi R C_f \rho_a (v_z - v_a)^2 + \rho g A + \pi s \frac{dR}{dz} \quad (5)$$

where ρ is the density of filament, $A = \pi R^2$ is the cross-sectional area of spinline, C_f is coefficient of friction drag, v_z, is the parallel air flow velocity that is in the opposite direction of v_z, ρ_a is the density of the gas phase, and s is the surface tension of the filament. The terms on the RHS of eq. (5) represent the forces of tension in the filament, air drag, gravity, and surface tension, respectively. The term on the LHS is the inertia.

Equation of energy

In deriving the energy balance equation for the 1D model, energy transport by radiation and energy conduction in the direction of the length of spinline are considered negligible. In addition, it is assumed that no crystallization occurs. Under these assumptions and combining the heat transfer boundary condition at the surface of the spinline, the energy equation becomes the following

$$\rho C_p v_z \frac{dT}{dz} = -\frac{2}{R}\left[h(T - T_a) + \Delta H_v k_y M_2 \frac{(a_2 P_2^{sat} - P y_{2_{s\infty}})}{(P - a_2 P_2^{sat})} \right] + (\tau_{zz} - \tau_{rr}) \frac{dv_z}{dz} \quad (6)$$

where C_p is the heat capacity of the polymer solution, h is the convective heat transfer coefficient, and ΔH_v is the heat of evaporation of the solvent per unit mass. The bracketed term on the RHS of the energy equation represents the combination of convective heat transfer between the filament and the quench air, and the evaporation of solvent. The second term on the right expresses the viscous heating.

A viscoelastic constitutive model

The viscosity of the spinning solutions is generally non-Newtonian, and can be influenced by factors such as molecular weight, concentration, temperature, and shear rate. Spinning solutions also exhibit elastic properties.[3] Schreiber et al.[15] and Hayahara et al.[16] have advocated that an elastically deformable entanglement network is formed at a critical solution concentration or molecular weight while preparing the spinning dope. It is believed by the authors that a similar entanglement network is also formed in the course of the dry spinning process. Leaving the spinneret, the spinning solution can be regarded as a "short range" entanglement network,[17] which means the low entanglement frequency because of the considerable existence of solvent would allow viscous flow before solidification or significant elastic strain. After a critical solution concentration, which may correspond to the solidification point, the filament becomes a "long range" entanglement network, which implies that a given polymer chain in the network is entangled with other chains at a sufficient number of points along its length. This drastically restricts the chain's random movement, thereby dramatically increasing its relaxation time. The long-range network has high viscosity because it possesses a certain amount of structural integrity. It is also elastically deformable if subject to a considerable magnitude of stress for the same reason. Therefore, a robust viscoelastic constitutive model is desirable to capture as many details of the observed

rheologic behavior and process dynamics of dry spinning as possible.

The Giesekus model is a realistic viscoelastic constitutive equation for both polymer melts and concentrated polymer solutions, which has successfully been used to predict material functions for shear and extensional flows.[18–20] In the case of melt spinning, the rheologic behavior of the amorphous phase (melt) is well represented by a modification of the single-mode Giesekus model, which takes into account the finite extensibility of the chains.[12] In the present study, the same modified Giesekus model is used, along with a relaxation time–concentration relationship for the dry spinning systems. In this model, the polymer solution is envisioned as a concentrated suspension of n nonlinear elastic dumbbell molecules per unit volume of solution. Each of the chains is assumed to contain N_o flexible statistical links of length l. The microstructure of the system is represented by the conformation tensor $\mathbf{c}$ characterizing the configurational state of the different kinds of network structures present in the concentrated solution.[18]

The extra stress tensor $\boldsymbol{\tau}$ for the spinning solution is expressed as

$$\boldsymbol{\tau} = nK_oE\mathbf{c} - G\boldsymbol{\delta} \tag{7}$$

where $\boldsymbol{\delta}$ is an identity tensor, K_o is the Hookean spring constant given by[21]

$$K_o = \frac{3k_BT}{N_ol^2}, \tag{8}$$

and the shear modulus is $G = nk_BT$, where k_B is the Boltzmann constant. E is a nonlinear spring force factor, which accounts for finite chain extensibility, and is given by[22]

$$E = \frac{L^{-1}(e)}{3e} \tag{9}$$

where L^{-1} is the inverse Langevin function, which is the function inverse to the Langevin function given by $L(x) = (\coth x) - x^{-1}$. The quantity e is defined as

$$e = \frac{(tr\mathbf{c})^{1/2}}{N_ol} \tag{10}$$

and represents the fractional extension of the chains, with the numerator being their length and the denominator being the contour length.

The $\mathbf{c}$ tensor can be obtained from the evolution equation[12,18,22]

$$\mathbf{c}_{(1)} = -\frac{1}{\lambda(T, w_1)}\frac{k_BT}{K_o}\left((1-\alpha)\boldsymbol{\delta} + \alpha\frac{K_o}{k_BT}E\mathbf{c}\right) \cdot \left(\frac{K_o}{k_BT}E\mathbf{c} - \boldsymbol{\delta}\right) \tag{11}$$

where the subscript (1) denotes the upper-convected derivative, and λ is a characteristic (Hookean) relaxation time of the polymer solution, α is the molecular (Giesekus) mobility parameter that lies in the range $0 \le \alpha \le 1$ and w_1 is the mass fraction of polymer. Note that λ here is dependent on not only temperature but also concentration. That is to say, the temperature and concentration dependences of the constitutive equation are contained in the relaxation time.

Although the shear modulus G would in general also be a function of temperature and concentration, the variation of modulus with temperature and concentration is generally much less pronounced than that of viscosity.[3] Thus, we assume that G is constant along the spinline and the relaxation time

$$\lambda = \frac{\eta_o(T, w_1)}{G} \tag{12}$$

is practically controlled by the zero-shear viscosity of the spinning solution, η_o, which is a function of polymer mass fraction w_1 and temperature T. It is anticipated that the viscosity of the filament in dry spinning would increase along with the polymer concentration, and more dramatically in the later stage when most of the solvent has evaporated. Unfortunately, it is experimentally difficult to obtain an accurate correlation of viscosity that covers the full range of concentration from semidilute to pure melt. On the other hand, we know from fundamental principles that for systems in the vicinity of their glass transition temperatures, the temperature dependence of the viscosity is well described by the familiar WLF (Williams-Landel-Ferry) equation[23]

$$\log a_T = \frac{-c_1(T - T_s)}{c_2 + (T - T_s)} \tag{13}$$

where a_T is the ratio of the relaxation times at temperature T and a standard temperature T_s, which has a certain relationship with glass transition temperature T_g. Because the relaxation time is related to the viscosity for a constant shear modulus, a_T can also be expressed as the viscosity ratio at the two temperatures. Likewise, for the Newtonian model, this same expression can be used to estimate the temperature and composition dependence of the viscosity. Diluents will, therefore, influence the temperature dependence of the viscosity and relaxation time primarily through their effect on T_g. One such dependence is the so-

TABLE I
Processing Conditions for Dry Spinning of CA/Acetone Used in the Simulations

Processing parameters	Values
Mass throughout, W	1.2 g/min
Mass fraction of solvent in the dope, w_{2o}	0.74
Spinneret hole diameter, d_o	0.0358 cm
Temperature at exit of spinneret, T_o	328.15 K
Air temperature, T_a	343.15 K
Total length of spinline, L_o	200 cm
Air flow out position, z_1	0 cm
Air flow in position, z_2	200 cm
Mole fraction of solvent vapor in air flow, $y_{2_{g^\infty}}$	0
Take up velocity, v_L	400 cm/s
Ambient pressure, P	1 atm
Velocity of parallel air flow, v_a	50 cm/s

called Kelley-Bueche equation, which has been shown to work well for a variety of glassy polymers.[24] The Kelley-Bueche equation predicts the glass transition temperature of binary polymer solutions as

$$T_g = \frac{R\phi_2 T_{g2} + \phi_1 T_{g1}}{R\phi_2 + \phi_1} \tag{14}$$

where T_{gi} are the pure component glass transition temperatures, and $R \equiv \alpha_2/\alpha_1$, with α_i being the difference in thermal expansivity between liquid and glass for component i. Theoretically, the solidification point of a glassy polymer is identified with the solvent concentration, which is sufficient to depress the glass transition of the polymer to the actual experimental temperature.

Material properties and input parameters

Cellulose acetate/acetone is convenient to use for illustration because it is a common dry spinning system for which most of the required material property data are available in the literature. The input parameters for our calculations based on this system are summarized in Tables I–II. Table I shows a typical set of processing parameters,[7] and Table II shows the physical and rheologic properties and typical model parameters.

Because rheologic data for CA/acetone are limited, typical values for the rheologic parameters are used from the literature. Although the simulation results are not sensitive to the number of statistical links per chain, N_o, a value of 100 was chosen since the relationship between N_o and the degree of polymerization P_n is unknown. Similar to the case for melt spinning,[12] the initial radial-to-axial stress ratio at the spinneret exit is assumed to be that for a Newtonian fluid and given by

$$R_s = \frac{\tau_{rr,o}}{\tau_{zz,o}} = \frac{Ec^*_{rr,o} - 1}{Ec^*_{zz,o} - 1} = -0.5. \tag{15}$$

Simulation results were found to be insensitive to R_s in the low take-up speed regime ($v_L < 1000$ cm/s).

Correlations for the material properties needed in the simulations are summarized below.

Viscosity of the CA/acetone system

The evaluation of solution viscosity basically involves three stages:[30]

1. For $T \geq T_s = 1.2\ T_g$, the temperature dependence of the zero-shear viscosity follows a simple exponential relationship as following:[7]

$$\eta_o = 6.6 \times 10^{-12} P_n^{3.7}(1 - w_2)^7 \exp(\Delta E/RT) \tag{16}$$

where η_o is given in poise, ΔE is the flow activa-

TABLE II
Physical and Rheologic Properties of CA/Acetone System

Properties	Values	References
Degree of polymerization of CA, P_n	200	—
Heat capacity of CA, C_{P1}	1.32×10^7 erg/(g K)	25
Partial specific volume of CA, $\hat{\nu}_1$	0.7634 cm^3/g	25
Molar volume of CA, V_1	31147 cm^3/gmol	25
Partial specific volume of acetone, $\hat{\nu}_2$	1.266 cm^3/g	25
Molar volume of acetone, V_2	73.53 cm^3/gmol	25
Critical temperature of acetone, T_c	508.1 K	26
Acentric factor of acetone, ϖ	0.304	26
Glass transition temperature of CA, T_{g1}	468 K	27
Glass transition temperature of acetone, T_{g2}	44 K	28
Number of statistical links per chain, N_o	100	—
Shear modulus, G	1.0×10^3 dyn/cm^2	29
Molecular weight of acetone, M_2	58.08 g/gmol	—
Molecular weight of air, M_a	28.97 g/gmol	—
Initial ratio of radial-to-axial stress, R_s	−0.5	—
Mobility parameter, α	0.1	—

tion energy with a typical value of 1.36×10^4 cal/mol, R is the universal gas constant, and T is in K.

2. For $T_g \leq T \leq T_s$, the WLF correlation eq. (13) is used as

$$\log \eta_o(T) = \log \eta_o(T_s) - \frac{c_1(T - T_s)}{c_2 + (T - T_s)} \quad (17)$$

where $c_1 = 8.86$ and $c_2 = 101.6$.

3. For $T \leq T_g$, the viscosity value at T_g is used.

The constants and properties used here are those given in van Krevelen[30] and shown in Table II.

Heat and mass transfer coefficients[7,31]

For the case of parallel air flow,

$$\mathrm{Nu} = 0.35 + 0.146(\mathrm{Re}_p + (1.03\ \mathrm{Re}_w^{0.36} - 0.685)^2)^{1/2} \quad (18)$$

where the Nusselt number $\mathrm{Nu} = 2Rh/k_a$, Re_p, and Re_w are Reynolds numbers based on the velocity of the parallel air flow, v_a and the running filament, v_L, respectively. Here, k_a is the thermal conductivity of the air. The gas-side mass transfer coefficient, k_y, is calculated using the assumed analogy between heat and mass transfer.[6] For acetone, an h/k_y value of 11.6 cal/(gmol K) estimated by Ohzawa et al.[7] is used.

Air drag coefficient[32]

$$C_f = 0.77\ \mathrm{Re}^{-0.61} \quad (19)$$

where

$$\mathrm{Re} = \frac{2R\rho_a|v_z - v_a|}{\eta_a},$$

ρ_a and η_a are the density and viscosity of the quench air, respectively.

Heat capacity [26]

For acetone,

$$C_{P2} = C^o_{P2} + R(1.45 + 0.45(1 - T_r)^{-1} + 0.25\bar{\omega}[17.11 + 25.2(1 - T_r)^{1/3}T_r^{-1} + 1.742(1 - T_r)^{-1}]) \quad (20)$$

where T_r is the reduced temperature, R is the universal gas constant, and C^o_{p2} is the heat capacity in the ideal-gas state at the same temperature, correlated as:

$$C^o_{P2} = 6.301 + 2.606 \times 10^{-1}T - 1.253 \times 10^{-4}T^2 + 2.038 \times 10^{-8}T^3. \quad (21)$$

The values of critical temperature T_c and acentric factor $\bar{\omega}$ of acetone are shown in Table II.

For CA, a constant value of heat capacity in Table II is used because good temperature-dependent correlations are lacking. Neglecting the effect of temperature on the heat of mixing gives the following for the mixture molar heat capacity,

$$C_p = (1 - \phi_2)C_{p1} + \phi_2 C_{p2} \quad (22)$$

Latent heat of evaporation of acetone[26]

$$\Delta H_v = RT_c\lfloor 7.08(1 - T_r)^{0.354} + 10.95\bar{\omega}(1 - T_r)^{0.456}\rfloor \quad (23)$$

Activity coefficient of acetone

The activity is evaluated from Flory-Huggins theory:[33]

$$a_2 = \phi_2 \exp\left[\phi_1\left(1 - \frac{V_2}{V_1} + \phi_1 g_{12} - \phi_1\phi_2\frac{dg_{12}}{d\phi_1}\right)\right] \quad (24)$$

where V_i is the molar volume of component i and CA–acetone interaction parameter g_{12} is estimated from[34]

$$g_{12} = 0.535 + 0.11\phi_1 \quad (25)$$

Vapor pressure of acetone[26]

The Antoine equation is used to estimate the vapor pressure of acetone as

$$P_2^{\mathrm{sat}} = \frac{1}{760}\exp\left[16.6513 - \frac{2940.46}{T - 35.93}\right] \quad (26)$$

where P_2^{sat} is given in atm.

Physical properties of quench air[12]

The density, viscosity, and thermal conductivity properties of the circulated air are approximated as

$$\text{Density: } \rho_a = 0.351/T_f\ (\mathrm{g/cm^3}) \quad (27)$$

$$\text{Viscosity: } \mu_a = \frac{1.446\times10^{-5}\mathrm{T_f^{1.5}}}{(\mathrm{T_f}+113.9)}(\text{poise}) \quad (28)$$

Thermal conductivity:

$$k_a = 4.49 \times 10^{-7}T_f^{0.866}(\mathrm{cal/(cms°C)}) \quad (29)$$

where T_f(K) is the film temperature defined as the arithmetic mean of the filament temperature and quench air temperature.

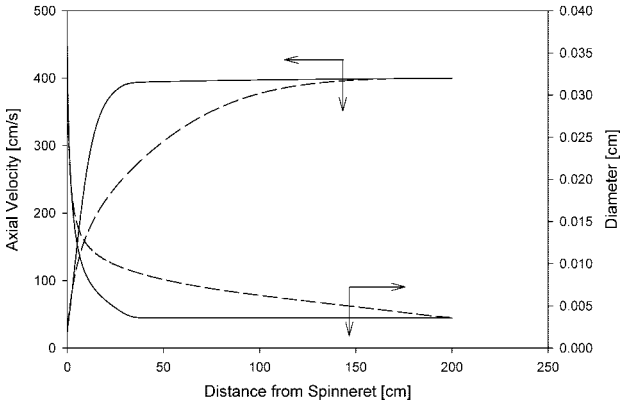

Figure 2 Comparison of computed axial velocity and diameter profiles along the spinline of Giesekus model with those of Newtonian model: (—) Giesekus model; (–) Newtonian model.

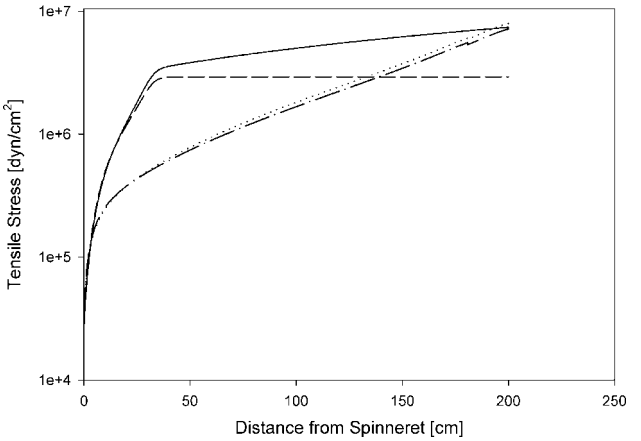

Figure 3 Comparison of computed tensile stress profiles along the spinline of Giesekus model with those of Newtonian model: (—) Giesekus with air drag and gravity; (–) Giesekus without air drag and gravity; (-·-) Newtonian with air drag and gravity; (···) Newtonian without air drag and gravity.

NUMERICAL METHOD

The dry spinning model consists of a system of strongly coupled differential equations in which the independent variables are v_z, ϕ_2, T, and tensor **c** (viscoelastic model) or dv_z/dz (Newtonian model). For computational efficiency, dimensionless variables and numbers are defined and the evolution equations are accordingly non-dimensionalized.[13] Those equations are solved as an initial value problem with a variable-step fourth order Runga-Kutta algorithm combined with a shooting method.[12] For the viscoelastic model, the algorithm proceeds as follows:

1. At $z = 0$, spinneret values are used for the initial velocity, temperature and concentration. A value of $c_{zz,o}$ is assumed and $c_{rr,o}$ is determined by eq. (15). The nonlinear force factor E is calculated iteratively using an initial value of 1.00.[35]
2. Implementing the fourth-order Runga-Kutta algorithm with a variable step results in the solution along the spin line from 0 to L_o. The calculated axial velocity at L_o is compared to the take-up speed v_L and the system is reiterated until the two match within a tolerance error of 0.1%.

For the Newtonian model, the algorithm goes in the same manner except dv_z/dz instead of c_{zz} is used in the shooting method as a trial variable.

RESULTS AND DISCUSSION

Comparison of constitutive models

Figure 2 shows a comparison of the spinline velocity and diameter profiles for the Newtonian and viscoelastic (Giesekus) models. One sees that the profiles for the viscoelastic model exhibit distinct plateaus, characteristic of fiber solidification, similar to that observed in low speed melt spinning.[12] The velocity increases sharply right after the spinneret and reaches a plateau equal to that of the take-up speed around a distance of 35 cm from the spinneret. Likewise, the diameter profile drops to a steady value around the same position that is then maintained to the take-up wheel. The velocity and diameter plateaus for the viscoelastic model reflect the fact that the stretchability of the filament decreases dramatically, leading to a lock-in of the system. By contrast, the Newtonian profile rises much less rapidly and appears to reach a plateau value at 150 cm downstream from the spinneret. However, as shown in Figure 3, the apparent plateau behavior for the Newtonian case is misleading because the stress does not lock in, instead rising monotonically to the value at the take-up wheel. Moreover, comparison of the profiles in the absence of gravity and air drag, also demonstrates that the grad-

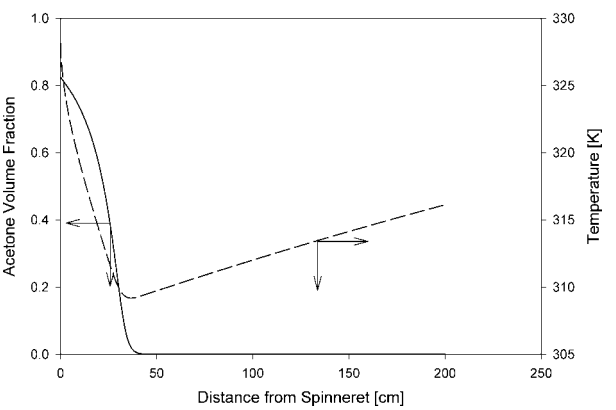

Figure 4 Calculated acetone composition and temperature profiles along the spinline of Giesekus model: (—) acetone volume fraction; (–) temperature.

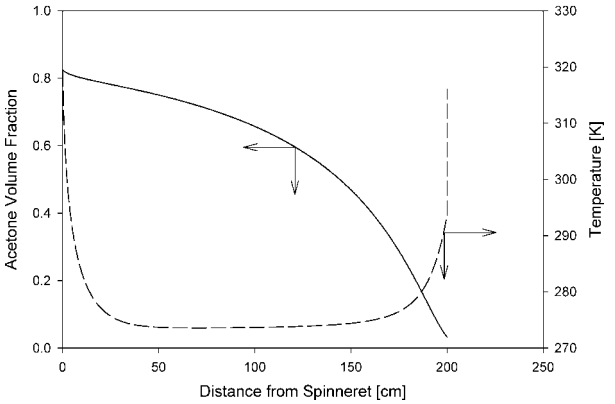

Figure 5 Calculated acetone composition and temperature profiles along the spinline of Newtonian model: (—) acetone volume fraction; (–) temperature.

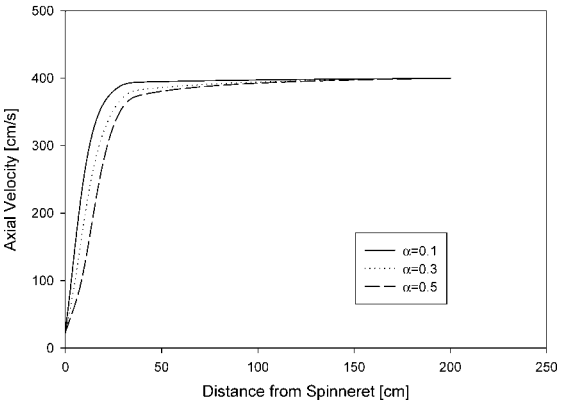

Figure 7 Effect of mobility parameter α on the axial velocity profile along the spinline.

ual rise of the stress to a final value at the take-up wheel is a reflection of the effects of gravity and air drag in the viscoelastic model. However, as seen, the Newtonian model does not exhibit a locking-in behavior, whereas the viscoelastic model does. Figure 3 also clearly illustrates that the assumption of constant tension along the spinline, commonly used in dry spinning models[6–8] is not realistic.

Insight on the reasons for these different patterns can be gained from the predicted temperature, composition, and viscosity profiles for the two models. As seen in Figure 4, solidification in the viscoelastic model corresponds to the point at which the acetone composition has dropped to zero and where the temperature profile has reached a local minimum. The large drop in the temperature profile near the spinneret reflects the endothermal effect of solvent vaporization [given by the second term in the square bracket in eq. (6)]. After the solidification point, the temperature rises and approaches that of the air temperature. Figure 5 shows that the temperature profile for the Newtonian model drops to an unrealistic point near 0°C, while the composition profile remains relatively high until near the take-up point. Figure 6 illustrates that the combination of lower temperature and less pronounced composition profiles in the Newtonian case, leads to a lower viscosity near the take-up; hence, the stresses do not lock-in. On the other hand, the zero-shear viscosity profile for the viscoelastic case, more rapidly rises to a glassy plateau, causing a sufficient increase in the relaxation time, to enable the system to lock-in (see Figs. 2 and 3).

Effect of mobility parameter α

The viscoelastic model introduces another parameter into the problem, namely that of the mobility parameter, α, which is basically a measure of the anisotropy of the molecular mobility of the melt. The limiting case $\alpha = 0$ corresponds to an isotropic mobility and leads to the constitutive equation of an upper-convected Maxwell model. The opposite limiting case $\alpha = 1$ corresponds to the most anisotropic mobility.[18] Normally one obtains this parameter from fits of the shear rate dependence of the solution viscosity and first normal stress or from fits of the extensional viscosity.[20] As

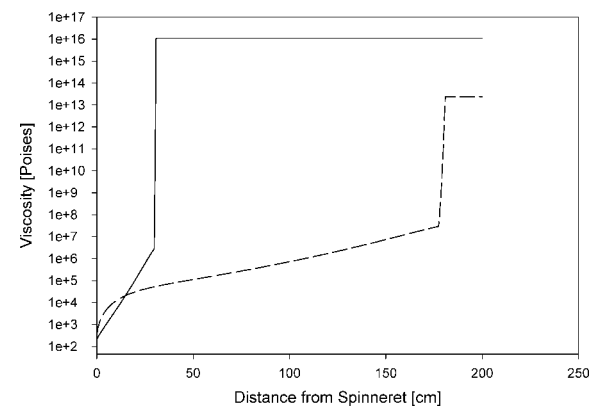

Figure 6 Comparison of computed zero-shear viscosity profiles along the spinline of Giesekus model with that of Newtonian model: (—) Giesekus; (–) Newtonian.

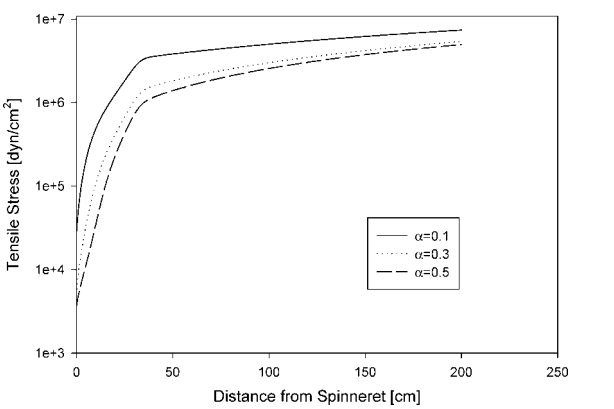

Figure 8 Effect of mobility parameter α on the tensile stress profile along the spinline.

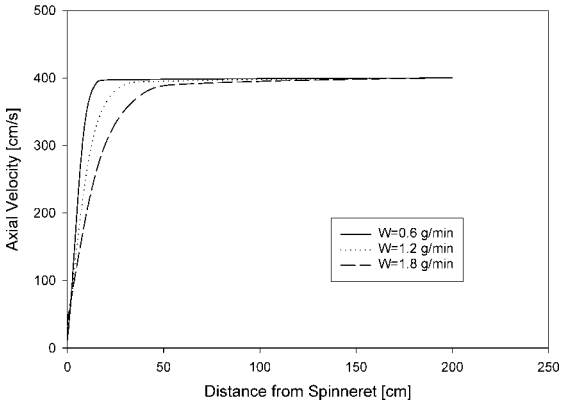

Figure 9 Effect of mass throughout W on the axial velocity profile along the spinline for the Giesekus model.

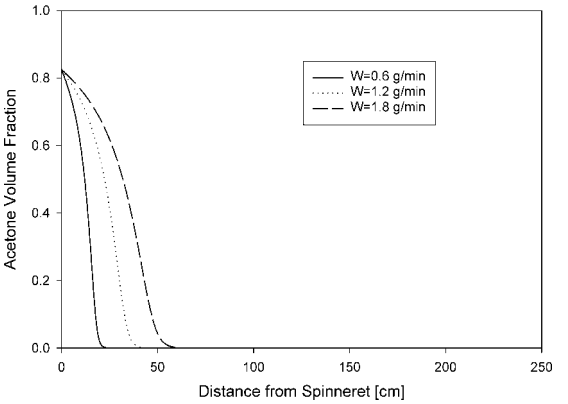

Figure 11 Effect of mass throughout W on the solvent concentration profile along the spinline for the Giesekus model.

shown in Figure 7, varying α over a range of 0.1 to 0.5, keeping all other parameters constant, results in a change of the exponential rise in the velocity; however, the plateau position remains more or less constant. The plateau also flattens slightly with decreasing α. These predictions suggest that α could be used as a model fitting parameter to adjust the velocity profile and improve the fit of experimental data around the solidification point. As seen in Figure 8, α has a more pronounced effect on the tensile stress. It is seen that tensile stress for $\alpha = 0.1$ starts from a larger value at the spinneret and increases very quickly to a much higher plateau compared with the case of $\alpha = 0.5$. The effect of α on the remaining profiles was found to be negligible.

Effects of processing conditions

The effects of mass throughout, take-up speed, air velocity, and vapor concentration for the viscoelastic model are described in this section. In all cases, the effect of a given processing condition is investigated keeping all other conditions and model parameters constant as shown in Tables I–II.

Sensitivity to variations of the mass flow rate was investigated over a wide range of throughout from 0.6 to 1.8 g/(min-capillary). With increasing mass flow rate, the final diameter plateau increases because of mass conservation; the deformation of the filament before solidification attenuates, and hence, the strain rate and tensile stress decrease accordingly (figure not shown); consequently, the solidification point shifts away from the spinneret as shown by the velocity profiles in Figure 9. Because of the variation of mass throughout, the temperature (Fig. 10) and solvent concentration (Fig. 11) profiles are also changed correspondingly, indicating the expected trend of the shifting of the solidification point further from the spinneret with increasing mass flow rate. Similar trends were observed with changes in the take-up speed in the range from 300 to 600 cm/s. Moreover, the filament tension is higher at higher take-up speeds, which is verified by the tensile stress profile (figure not shown). Likewise, the effect of air velocity is very similar to that of take-up speed for the temperature, solvent concentration, strain rate, and tensile stress profiles,

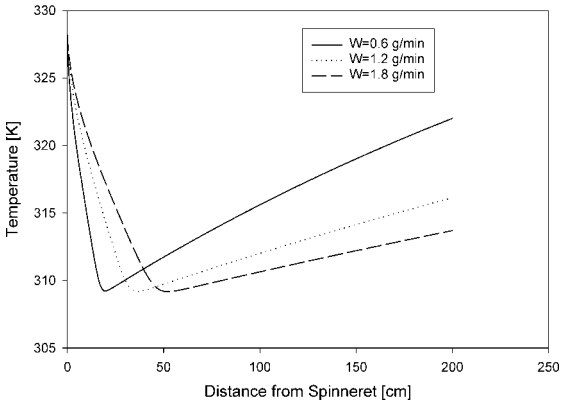

Figure 10 Effect of mass throughout W on the temperature profile along the spinline for the Giesekus model.

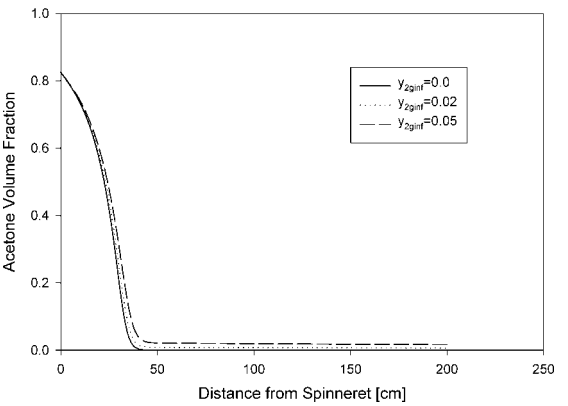

Figure 12 Effect of vapor composition on the solvent concentration profile along the spinline for the Giesekus model. Here, $y_{2\mathrm{ginf}}$ is the same as $y_{2g^{\infty}}$ shown in Figure 1.

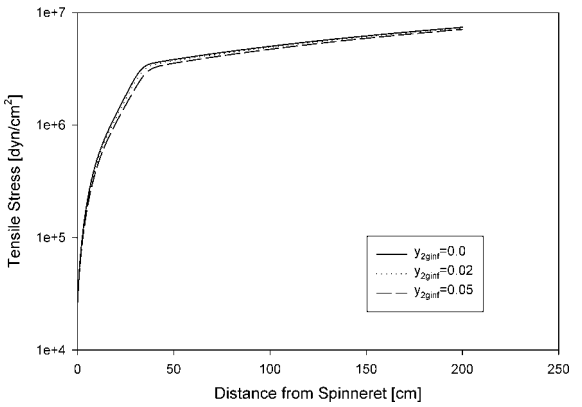

Figure 13 Effect of vapor composition on the tensile stress profile along the spinline for the Giesekus model. Here, $y_{2\mathrm{ginf}}$ is the same as $y_{2g\infty}$ shown in Figure 1.

while the effects on velocity and diameter profiles are small (figures not shown).

The effect of residual solvent in the air flow on the concentration profile shown in Figure 12 is not surprising because, due to evaporation, the concentration inside the filament approaches the equilibrium value associated with the given ambient concentration. Moreover, the tensile stress decreases slightly due to the residual solvent inside the filament as shown in Figure 13.

CONCLUSIONS

The results of our model calculations for dry spinning based on Newtonian and modified Giesekus constitutive equations for the spinning solution, suggest the importance of viscoelasticity in the fiber solidification along the spinline. The discussion of the effect of mobility parameter α suggests that α could be used as a model fitting parameter to adjust the velocity profile and improve the fit of experimental data around the solidification point. The effects of mass throughout, take-up speed, air velocity, and vapor concentration are also investigated and this makes possible to link processing conditions with final product properties and serve as a useful tool for process optimization.

This work has been supported in part by the ERC program of the National Science Foundation under Award No. EEC-9731680 administered through the Center for Advanced Engineering Fibers and Films at Clemson University, and in part by a grant from Celanese Acetate Company.

References

1. Gogolewski, S.; Pennings, A. J Polym 1985, 26, 1394.
2. Leenslag, J. W.; Pennings, A. J Polym 1987, 28, 1695.
3. Ziabicki, A. Fundamentals of Fibre Formation; Wiley: New York, 1976.
4. Fok, S. Y.; Griskey, R. G. Appl Sci Res 1966, 16, 141.
5. Fok, S. Y.; Griskey, R. G. J Appl Polym Sci 1967, 11, 2417.
6. Ohzawa, Y.; Nagano, Y.; Matsuo, T. J Appl Polym Sci 1969, 13, 257.
7. Ohzawa, Y.; Nagano, Y. J Appl Polym Sci 1970, 14, 1879.
8. Ohzawa, Y.; Nagano, Y.; Matsuo, T. Proceedings of the 5th International Congress on Rheology. University Park Press: Baltimore, MD, 1970, p. 393, vol. 4.
9. Brazinsky, I.; Williams, A. G.; LaNieve, H. L. Polym Eng Sci 1975, 15, 834.
10. Ishihara, H.; Tani, K.; Hayashi, S.; Ikeuchi, H. J Polym Eng 1986, 6, 237.
11. Zhou, J. Ph D Thesis, the University of Tennessee, Knoxville, 1996.
12. Doufas, A. K.; McHugh, A. J.; Miller, C.; Immaneni, A. J Non-Newtonian Fluid Mech 2000, 92, 27.
13. Gou, Z. M S Thesis, University of Illinois, Urbana, 2001.
14. Vasudevan, G.; Middleman, S. AIChE J 1970, 16, 614.
15. Schreiber, H. P.; Rudin, A.; Bagley, E. B. J Appl Polym Sci 1965, 9, 887.
16. Hayahara, T.; Takao, S. J Appl Polym Sci 1965, 11, 735.
17. Griswold, P. D.; Cuculo, J. A. J Appl Polym Sci 1974, 18, 2887.
18. Giesekus, H. J Non-Newtonian Fluid Mech 1982, 11, 69.
19. Bird, R. B.; Curtis, C. F.; Armstrong, R. C.; Hassager, O. Dynamics of Polymeric Liquids; Wiley: New York, 1987, vol. 1.
20. Wiest, J. M. Rheol Acta 1989, 28, 4.
21. Bird, R. B.; Curtis, C. F.; Armstrong, R. C.; Hassager, O. Dynamics of Polymeric Liquids; Wiley: New York, 1987, vol. 2.
22. Peterlin, A. Pure Appl Chem 1966, 12, 563.
23. Ferry, J. D. Viscoelastic Properties of Polymers; Wiley: New York, 1980, 3rd ed.
24. Kelley, F. N.; Bueche, F. J Polym Sci 1961, 50, 549.
25. Brandrup, J.; Immergut, E. H.; Grulke, E. A.; Abe, A.; Bloch, D. R. Polymer Handbook; Wiley: New York, 1999, 4th ed.
26. Reid, R. C.; Prausnitz, J. M.; Sherwood, T. K. The Properties of Gases and Liquids; McGraw-Hill: New York, 1977, 3rd ed.
27. http://www.celaneseacetate.com/filament/why_acetate/fb-4.shtml.
28. Barton, B. F.; McHugh, A. J. J Polym Sci Part B Polym Phys 1999, 37, 1449.
29. Uchiyama, S. Sen-i Gakkaishi 1966, 22, 365.
30. van Krevelen, D. W. Properties of Polymers; Elsevier: Amsterdam, 1990, 3rd ed.
31. Sano, Y.; Yamada, N. Kagaku Kogaku 1966, 30, 997.
32. Shimizu, J.; Okui, N.; Tamai, K. Sen-I Gakkaishi 1983, 39, 62.
33. Tsay, C. S.; McHugh, A. J. J Polym Sci Part B Polym Phys 1990, 28, 1327.
34. Yilmaz, L.; McHugh, A. J. J Appl Polym Sci 1986, 31, 997.
35. Doufas, A. K.; Dairanieh, I. S.; McHugh, A. J. J Rheol 1999, 43, 85.